EUROPEAN ORGANIZATION FOR NUCLEAR RESEARCH

L3 Note 2571
July 6, 2000

Analysis of the $\pi^+\pi^-\pi^+\pi^-$ final state in $\gamma\gamma$ collisions at LEP

The L3 Collaboration

Abstract

The reaction $\gamma\gamma \rightarrow \pi^+\pi^-\pi^+\pi^-$ is studied with the L3 detector at LEP. The data sample was collected by L3 at centre-of-mass energies from 160 GeV to 202 GeV with a total integrated luminosity of 466.2 pb^{-1}. The process is dominated by $\rho^0\rho^0$ production. A spin-parity analysis of the $\rho^0\rho^0$ system for $W_{\gamma\gamma} < 3$ GeV shows a dominance of $J^P = 2^+$ and helicity 2. A contribution of $J^P = 0^+$ is also observed whereas contributions of negative parity states and $(J^P, J_z) = (2^+, 0)$ are found to be negligible. For the $\gamma\gamma$ mass region $W_{\gamma\gamma} > 3$ GeV the $f_2(1270)$ meson is also observed in the data.

Submitted to the
XXXth International Conference on High Energy Physics
Osaka, Japan, July 27 - August 2, 2000

1 Introduction

A large cross section for the two-photon reaction $\gamma\gamma \to \rho^0\rho^0$ near threshold has been observed in several experiments [1] - [7]. The cross section exceeds the estimations from the vector dominance model (VDM) by almost one order of magnitude. Similar enhancements have been also found in the decay $J/\psi \to \gamma\rho\rho$ [8] and in inelastic anti-proton scattering on deuterium $\bar{p}d \to \pi^-(2\pi^+2\pi^-)$ [9].

In contrast to $\rho^0\rho^0$ production the cross section for the isospin related reaction $\rho^+\rho^-$ was shown to be small [10] - [11]. The ratio of these cross sections is approximately equal to $\sigma(\gamma\gamma \to \rho^0\rho^0)/\sigma(\gamma\gamma \to \rho^+\rho^-) \approx 4$.

There exist a number of theoretical attempts to describe these experimental results. In a t-channel factorization approach [12], the $\rho^0\rho^0$ cross section is related to photo-production and the hadronic cross section at low energies. This model leads to the interpretation of the broad enhancement in the $\rho^0\rho^0$ cross section around 1.6 GeV as a threshold behaviour due to Regge exchange. Other models suggest an intermediate $\rho^0\rho^0$ resonance [13] - [14], either a normal $q\bar{q}$ state or a four-quark $qq\bar{q}\bar{q}$ bound state. In four-quark models, isoscalar and isotensor resonances interfere destructively to suppress the $\rho^+\rho^-$ signal and constructively to reproduce well the $\rho^0\rho^0$ cross section. The proposed models differ substantially in the predicted cross section for pair production of other vector mesons e.g. $\gamma\gamma \to \rho^0\omega$, $\gamma\gamma \to \phi\phi$.

If the enhancement for the cross section $\gamma\gamma \to \rho^0\rho^0$ is due to resonance production, the final state would have well defined spin and parity.

For the first time a spin-parity-helicity analysis for the reaction $\gamma\gamma \to \pi^+\pi^-\pi^+\pi^-$ was carried out by the TASSO Collaboration [3] by studying angular correlations in the four pion final state. The data sample consisted of 1722 events in the region $1.2 < M_{4\pi} < 2.0$ GeV. A spin-parity-helicity analysis with higher statistics was done by ARGUS Collaboration [7]: 5181 events were analysed in the four pion mass region between 1.1 and 2.3 GeV. Both groups used similar models and found the dominance of the $\rho^0\rho^0$ state $(J^p, J_z) = (2^+, 2)$ with a small contribution from the 0^+ state. The contribution of the negative parity states is found to be negligible.

In this paper the results of the spin-parity-helicity analysis of the reaction $\gamma\gamma \to \pi^+\pi^-\pi^+\pi^-$ for the data collected by the L3 detector at LEP are presented using the same model as TASSO and ARGUS.

2 Monte Carlo

To produce four pion events we use the Monte-Carlo generator EGPC [15]. The four-momentum of the $\gamma\gamma$ system is generated according to the $\gamma\gamma$ transverse luminosity function [16]. The generation of pion four-momentum vectors is performed according to four particle phase space. At present the Monte Carlo statistics is 2.5 times smaller than data. The $\gamma\gamma \to$ *hadrons* processes are simulated with the PHOJET [1)] [17] and PYTHIA [2)] [18]. The generated events are passed through the full L3 detector simulation using the GEANT [19] and GEISHA [20] programs and are reconstructed following the same procedure used for the data. A trigger simulation is also performed.

[1)] PHOJET version 1.05c
[2)] PYTHIA version 5.718 and JETSET version 7.408

3 Event Selection

The two-photon production of four pions, $\gamma\gamma \rightarrow \pi^+\pi^-\pi^+\pi^-$ is observed via the reaction $e^+e^- \rightarrow e^+e^-\pi^+\pi^-\pi^+\pi^-$. Detection of the scattered e^+ or e^- is not required in this analysis (no-tag events). Data have been collected during 1996–1999 with the L3 detector at e^+e^- centre-of-mass energies $\sqrt{s}$=160 – 202 GeV with a total integrated luminosity of $\mathcal{L}$ = 466.2 pb^{-1}. The L3 detector has been described elsewhere [21]. The analysis described in this paper is mainly based on the central tracking system.

The events are collected by a TEC track trigger [22], which requires at least two charged particles with $p_t > 150$ MeV, back to back, in the plane transverse to the beam within $\pm 60^0$ and a inner TEC trigger [23], which based on a neural network, trained to select low multiplicity events but reject beam-gas and beam-wall events.

In order to select $\gamma\gamma \rightarrow \pi^+\pi^-\pi^+\pi^-$ events, we require:

- Exactly four charged tracks in the tracking chamber with a net charge of zero. A track requires more than 12 hits out of a maximum of 62. The tracks must come from the primary vertex inside 3σ of the experimental detector resolution both in the transverse plane and along the beam axis. The experimental resolutions depend on the transverse momentum and on the length of the tracks.

- Events with photons are rejected. A photon is defined as an isolated shower in the electro-magnetic calorimeter with an energy greater than 100 MeV and with no nearby track within 200 mrad.

- Pion identification is based on the dE/dx information. The energy loss dE/dx must correspond to the hypotheses of four pions with a confidence level CL(4π) > 6%.

To suppress the background from non-exclusive four-track events we require the net transverse momentum $P_T^2 \equiv (\Sigma \vec{p}_T)^2$ to be smaller than 0.02 GeV^2.

After applying these cuts a sample of 56359 events is obtained, of which 55120 events lie in the mass region between 1.0 and 3.0 GeV. The mass distribution of the four pions final states is shown in Fig. 1. A steep rise at the $\rho^0\rho^0$ threshold $M_{4\pi} \approx 1.2$ GeV and a broad maximum $M_{4\pi} \approx 1.6$ GeV is clearly seen.

4 Two Pion Mass Spectra

We divide our data sample in two parts low mass data ($W_{\gamma\gamma} < 3.0$ GeV) and high mass data ($W_{\gamma\gamma} > 3.0$ GeV). The spin-parity and helicity analysis is performed only on the low mass data. The high mass sample is compared to Monte Carlo predictions.

4.1 Low $\gamma\gamma$ Mass Region

For a final state of four charged pions, there are four unlike-sign $\pi^+\pi^-$ combinations and two like-sign $\pi^\pm\pi^\pm$ combinations. Fig. 2 shows, on the left the scatter plots of the unlike-sign combinations, with four entries per event, for different $M_{4\pi}$ intervals. The corresponding like-sign combinations (two entries per event) are given on the right. The mass distribution of the unlike-sign combinations exhibit a clear ρ^0 signal, centred of the ρ^0 mass, for the $W_{\gamma\gamma}$ well above the $\rho^0\rho^0$ threshold. For $W_{\gamma\gamma} < 1.6$ GeV the ρ^0 signal is distorted by threshold effects.

M_ρ MeV	Γ_ρ MeV
765±3 MeV	129±7 MeV
M_{f_2} MeV	Γ_{f_2} MeV
1261±9 MeV	217 ± 28 MeV
M_X MeV	Γ_X MeV
1883 ± 35 MeV	911 ± 68 MeV

Table 1: Mass and width for ρ^0 and f_2-resonances obtained by a three Breit-Wigner fit on the high-mass data ($W_{\gamma\gamma} > 3$ GeV).

The background like-sign combinations show very different shapes for the all intervals of the $\gamma\gamma$ mass.

4.2 High $\gamma\gamma$ Mass Region

Fig. 3 shows similar scatter plots for $W_{\gamma\gamma} > 3.0$ GeV. We use like-sign combinations to estimate the level of combinatorial background under the unlike-sign distribution. The $\pi^+\pi^-$ mass spectrum after subtraction of the $\pi^\pm\pi^\pm$ combinatorial background is presented in Fig. 4. There is still a strong production of the ρ^0 meson but the $f_2(1270)$ meson is also seen. A fit to this spectrum with three Breit-Wigner functions gives mass and width of the ρ^0 and of the $f_2(1270)$ in very good agreement with PDG [24] values (Table 1).

Comparison of the data with Monte Carlo predictions are shown in Fig. 5 for the PYTHIA Monte Carlo generator and in Fig. 6 for the PHOJET Monte Carlo generator. For both MC-generators a peak in the ρ^0 mass region ($M_\rho^0 = 770$ MeV) is visible. But neither PYTHIA nor PHOJET is able to predict the $f_2(1270)$ resonance and the enhancement at higher masses.

Since the f_2 is a tensor meson $I^G(J^{PC}) = 0^+(2^{++})$ it cannot be produced diffractively because its quantum numbers differ from the ones of the photon. One possibility to produce the f_2 meson is an intermediate resonance decaying into a pair of f_2 mesons : $\gamma\gamma \to R \to f_2 f_2$. Additional studies are needed to clarify this hypotheses.

5 Spin-Parity-Helicity Analysis

According to the model proposed by TASSO [3] in the analysis of the reaction $\gamma\gamma \to \pi^+\pi^-\pi^+\pi^-$ we consider the $\rho^0\rho^0$ production in different spin-parity and helicity states (J^P, J_z) and isotropic production of $\rho^0\pi^+\pi^-$ and $\pi^+\pi^-\pi^+\pi^-$. All states are assumed to be produced incoherently and therefore no interference effects between these three final states are taken into account. The analysis is performed in intervals of $W_{\gamma\gamma}$ of 50 MeV. Since pions are bosons, the amplitude which describes the process must be symmetric under interchange of two pions with the same charge. The appropriate amplitudes satisfying these requirements are:

$$g_{\rho^0\rho^0} = BW(m_{\rho_1^0})BW(m_{\rho_2^0})\Psi_{J^P J_z}(1,2) + \text{permutations}$$
$$g_{\rho^0\pi^+\pi^-} = BW(m_{\rho_1^0}) + \text{permutations}$$
$$g_{4\pi} = 1$$

where $BW(m_{\rho^0})$ is the relativistic Breit-Wigner amplitude for the ρ^0 meson [25] and Ψ_{J^P,J_z} is the angular part of amplitude which describe the rotational properties of the $\rho^0\rho^0$ state with definite spin-parity J^P and helicity J_z. It is constructed by combining the spin of the two ρ^0 mesons $\vec{S} = \vec{s}_1 + \vec{s}_2$ and by adding the orbital angular momentum $\vec{L}$ to obtain the state with total spin $\vec{J}$:

$$\Psi_{J^P J_z LS} = \sum_{M,m_1} C^{J^P J_z}_{LMSM_s} C^{SM_s}_{s_1 m_1 s_2 m_2} Y_{LM}(\xi_1) Y_{s_1 m_1}(\xi_2) Y_{s_2 m_2}(\xi_3)$$

where $\xi_1 = (\vartheta_\rho, \varphi_\rho), \xi_2 = (\vartheta_{\pi_1^+}, \varphi_{\pi_1^+})$ and $\xi_3 = (\vartheta_{\pi_2^+}, \varphi_{\pi_2^+})$. $\vartheta_\rho, \varphi_\rho$ are the polar and the azimuthal angles of the ρ^0 meson in the $\gamma\gamma$ helicity system. The z axis is chosen parallel to the beam direction, which in good approximation, is parallel to the $\gamma\gamma$ helicity axis. The angles $\vartheta_{\pi_1^+}, \varphi_{\pi_1^+}$ $(\vartheta_{\pi_2^+}, \varphi_{\pi_2^+})$ are the polar and azimuthal angles of positive pions in the center-of-mass of the first (second) ρ^0 meson with z axis parallel to the beam axis. Since the analysis is performed close to threshold, the orbital angular momenta are restricted to $L = 0, 1$. The allowed spin-parity-helicity final states of the $\rho^0\rho^0$ system in quasi-real $\gamma\gamma$ reactions are : $(J^P, J_z) = 0^+, (2^+, 0), (2^+, \pm 2), 0^-$ and $(2^-, 0)$ with total spin of the $\rho^0\rho^0$ meson system $S = 1$ or $S = 2$. Other states are forbidden by helicity conservation or by the Landau-Yang theorem [26].

In each $W_{\gamma\gamma}$ bin a maximum likelihood fit is used to determine the contribution λ_j of the eight amplitudes to the data sample. The fit maximizes the logarithm of the likelihood function:

$$\log \Lambda = \sum_{i=1}^{N} \left[\log\Big(\sum_j \lambda_j \frac{|g_j(\xi_i)|^2}{\overline{|g_j|^2}} \Big) - \sum_j \lambda_j \right]$$

with the constraint:

$$\sum_j \lambda_j = 1 \quad ,$$

where N is the number of events in the bin. The average of the square of the amplitude is :

$$\overline{|g_j|^2} \equiv \int d\xi R_4(W_{\gamma\gamma}, \xi) |g_j(\xi)|^2 A(W_{\gamma\gamma}, \xi),$$

here R_4 is the four particle phase space factor and $A(W_{\gamma\gamma}, \xi)$ is the detector acceptance. The acceptance $A(W_{\gamma\gamma}, \xi)$ is independent of the process considered. The Monte Carlo selected events are used to compute the integral. The symbol ξ represents the set of seven variables needed to describe the four particles final state:

$$\xi = (m_{12}^2, m_{34}^2, \theta_\rho^{12}, \theta_\pi^{12}, \phi_\pi^{12}, \theta_\pi^{34}, \phi_\pi^{34}) \quad ,$$

the numbers from 1 to 4 refer to the four pions using the convention: $\pi_1^+ \pi_2^- \pi_3^+ \pi_4^-$. The variables m_{ij} denotes the mass of two pion combination i and j and the angles are defined above.

To test the fitting procedure event samples with mixtures of the various processes were obtained by re-weighting the events generated according to the phase space distribution with appropriate weight $|g_j|^2$. The fit reproduces the input mixture within statistical errors.

The cross section for the process j, averaged over the $W_{\gamma\gamma}$ bin is calculated using the following formula:

$$\sigma_{\gamma\gamma\to k} = \frac{N\lambda_k}{\mathcal{L}_{\mathrm{e^+e^-}}\ \varepsilon(W_{\gamma\gamma})\ \varepsilon_{trg}(W_{\gamma\gamma})\ \frac{\Delta\mathcal{L}_{\gamma\gamma}}{\Delta W_{\gamma\gamma}}\ \Delta W_{\gamma\gamma}} \quad ,$$

where N is the number of events in the $\Delta W_{\gamma\gamma}$ bin, $\mathcal{L}_{\mathrm{e^+e^-}}$ is the integrated $\mathrm{e^+e^-}$ luminosity and $\frac{\Delta\mathcal{L}_{\gamma\gamma}}{\Delta W_{\gamma\gamma}}$ is the differential $\gamma\gamma$ luminosity function, $\varepsilon(W_{\gamma\gamma})$ is the acceptance and selection efficiency and $\varepsilon_{trg}(W_{\gamma\gamma})$ is the trigger efficiency.

The selection efficiencies depend on the model and on the $W_{\gamma\gamma}$. They are computed by Monte Carlo, re-weighting the generated and accepted events with $|g_j|^2$. Fig. 7 shows the selection efficiency for the three isotropic production of $\rho^0\pi^+\pi^-$, $\pi^+\pi^-\pi^+\pi^-$ and $\rho^0\rho^0$ final states and for the six different spin-parity-helicity $\rho^0\rho^0$ final states.

The trigger inefficiency is studied separately for each year's data sample by comparing the response of the inner TEC trigger to the response of outer TEC trigger. The higher level triggers are studied with prescaled rejected events. In the relevant kinematic range of $W_{\gamma\gamma}$ the trigger efficiency is $W_{\gamma\gamma}$ mass dependent and it varies typically between 0.86 at 1 GeV and 0.90 at 3 GeV.

The cross sections derived from the eight parameter fit are shown in Fig. 8. The $\rho^0\rho^0$ state with spin-parity 2^+ and helicity 2 dominates. The $J^P = 0^+$ state is also significant in the $\gamma\gamma$ mass region from 1.3 GeV to 2. GeV. The contributions of the negative parity states and of the state with $(2^+, 0)$ are negligible. These results agree well with ARGUS [7] analysis.

To check the stability of the fit and the possible migration of the events between different states the fit is repeated with only the four significant states: $\pi^+\pi^-\pi^+\pi^-$, $\rho^0 2\pi$ and $\rho^0\rho^0$ with $(J^p, J_z) = 0^+, (2^+, 2)$. Similar cross-sections are obtained.

To demonstrate how this model describes the data we compare the angular distributions of the data with Monte Carlo simulation. The opening angle ϑ between the directions of two positive charge pions and the angle χ between the two ρ^0 decay planes are plotted on Fig. 9 for the $1.3 < W_{\gamma\gamma} < 1.5$ GeV and on Fig. 10 for the $1.6 < W_{\gamma\gamma} < 1.8$ GeV. Two entries per event are made due to permutation of particles. The raw data, before efficiency corrections, are plotted as points. The distributions of the individual waves and of the eight parameter fit (solid line) are obtained with Monte Carlo simulation at the reconstructed event level. From this plots it is clear that the data is rather well described.

6 Conclusions

The high statistics sample of $e^+e^- \rightarrow e^+e^-\pi^+\pi^-\pi^+\pi^-$, obtained by L3 at LEP confirms the dominance of the $\rho^0\rho^0$ $(2^+, 2)$ state below 2 GeV. The 0^+ wave is also present, while contribution from negative parity states are found to be negligible. More study is necessary to establish the resonance nature of the observed waves. For the high mass data $W_{\gamma\gamma} > 3$ GeV, together with ρ^0 production, an importante $f_2(1270)$ production is also observed.

References

[1] TASSO Coll., R. Brandelik *et al.*, *Phys. Lett.* **97 B** (1980) 448.

[2] MARK II Coll., D.L. Burke *et al.*, *Phys. Lett.* **103 B** (1981) 153.

[3] TASSO Coll., M. Althoff *et al.*, *Z. Phys.* **C 16** (1982) 13.

[4] CELLO Coll., H.-J. Behrend *et al.*, *Z. Phys.* **C 21** (1984) 205.

[5] PLUTO Coll., Ch. Berger *et al.*, *Z. Phys.* **C 38** (1988) 521.

[6] TPC/Two-Gamma Coll., H. Aihara *et al.*, *Phys. Rev.* **37 D** (1988) 28.

[7] ARGUS Coll., H. Albrecht *et al.*, *Z. Phys.* **C 50** (1991) 1.

[8] MARK III Coll., R.M.Baltrusaitis *et al.*, *Phys. Rev.* **D 33** (1986) 1222.

[9] D. Bridges *et al.*, *Phys. Rev. Lett.* **56** (1986) 211;
D. Bridges *et al.*, *Phys. Rev. Lett.* **56** (1986) 215.

[10] JADE Coll., J.E. Olsson *et al.*, Proc. of the 5^{th} Int. Colloquium on $\gamma\gamma$-Interactions, Aachen, p. 45; ed. Ch. Berger, Lectures Notes in Physics, Vol. 191, Springer Verlag (1983).

[11] ARGUS Coll., H. Albrecht *et al.*, *Phys. Lett.* **217 B** (1989) 217.

[12] G. Alexander, U. Maor, P.G. Williams, *Phys. Rev.* **D 26** (1982) 1198;
G. Alexander, A. Levy, U. Maor, *Z. Phys.* **C 30** (1986) 65.

[13] Bing An Li, K.F. Liu, *Phys. Lett.* **118 B** (1982) 435 ;
Bing An Li, K.F. Liu, *Erratum Phys. Lett.* **124 B** (1983) 550;
Bing An Li, K.F. Liu, *Phys. Rev. Lett.* **51** (1983) 1510;
Bing An Li, K.F. Liu, *Phys. Rev.* **D 30** (1984) 613;
Bing An Li, K.F. Liu, *Phys. Rev. Lett.* **58** (1987) 2288.

[14] N.N. Achasov *et al.*, *Phys. Lett.* **108 B** (1982) 134;
N.N. Achasov *et al.*, *Z. Phys.* **C 16** (1982) 55;
N.N. Achasov *et al.*, *Z. Phys.* **C 27** (1985) 99;
N.N. Achasov *et al.*, *Phys. Lett.* **203 B** (1988) 309.

[15] F. L. Linde "Charm Production in Two-Photon Collision", Ph. D. Thesis, Rijksuniversiteit Leiden, (1988).

[16] V. M. Budnev *et al.*, *Phys. Rev.* **C 15** (1975) 181.

[17] R. Engel, *Z. Phys.* **C 66** (1995) 203;
R. Engel and J. Ranft, *Phys. Rev.* **D 54** (1996) 4246;

[18] T. Sjöstrand, *Comput. Phys. Commun.* **82** (1994) 74.

[19] R. Brun *et al.*, GEANT 3.15 preprint CERN DD/EE/84-1 (Revised 1987).

[20] H. Fesefeldt, RWTH Aachen report PITHA 85/2 (1985)

[21] L3 Coll., B. Adeva *et al.*, *Nucl. Inst. Meth.* **A 289** (1990) 35;
M. Acciari *et al.*, *Nucl. Inst. Meth.* **A 351** (1994) 30.

[22] P. Béné et al., *Nucl. Inst. Meth.* **A 306** (1991) 150.

[23] D. Haas et al., *Nucl. Inst. Meth.* **A 420** (1999) 101.

[24] Particle Data Group, C.Caso *et al.*, *Eur. Phys. J.* **C 3** (1988) 1.

[25] J.D. Jackson, *Nuovo Cimento* **34**, (1964) 1644.

[26] L. D. Landau, Dokl. Akad. Nauk (USSR) 60 (1948) 207 (english summary in Phys. Abstracts **A 52** (1949),125);
C. M. Yang, *Phys. Rev.* **77** (1950) 242.

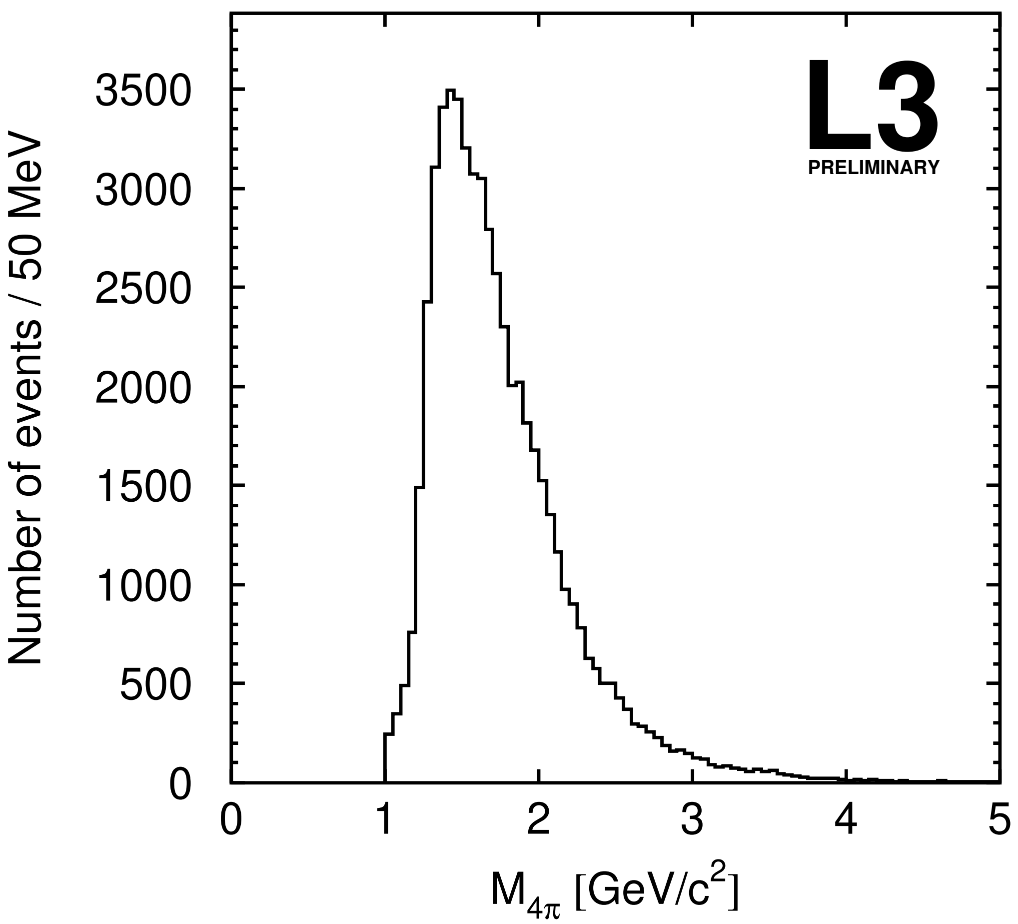

Figure 1: Mass distribution of the four pions for $e^+e^- \rightarrow e^+e^-\pi^+\pi^-\pi^+\pi^-$ events after selection cut $(\Sigma\vec{p}_T)^2 < 0.02$ GeV^2.

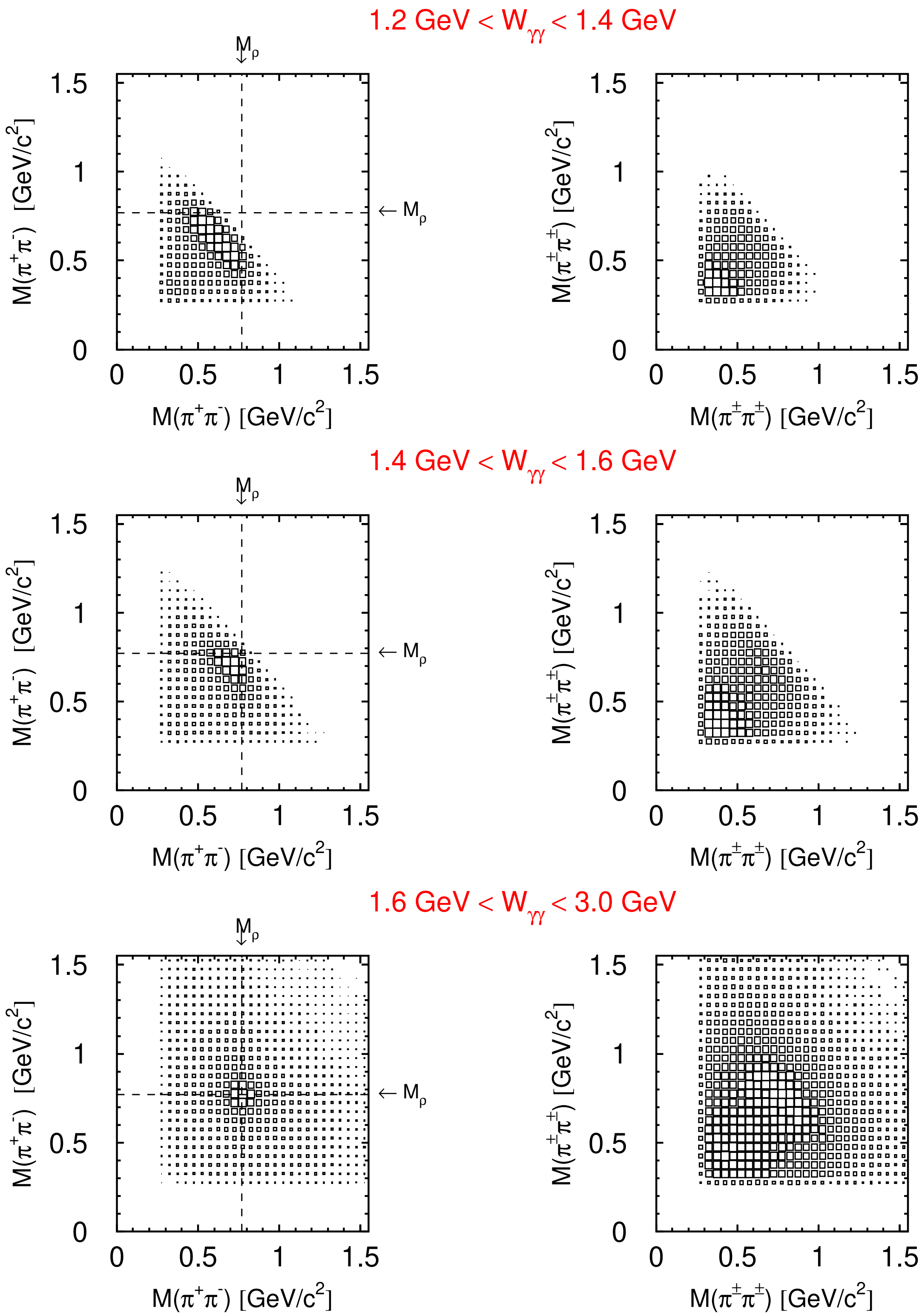

Figure 2: Scatter plots of two pion mass distribution, on the left for unlike-sign charge ($\pi^+\pi^-$) combinations (four entries per event) and on the right for like-sign charge ($\pi^\pm\pi^\pm$) mass combinations (two entries per event).

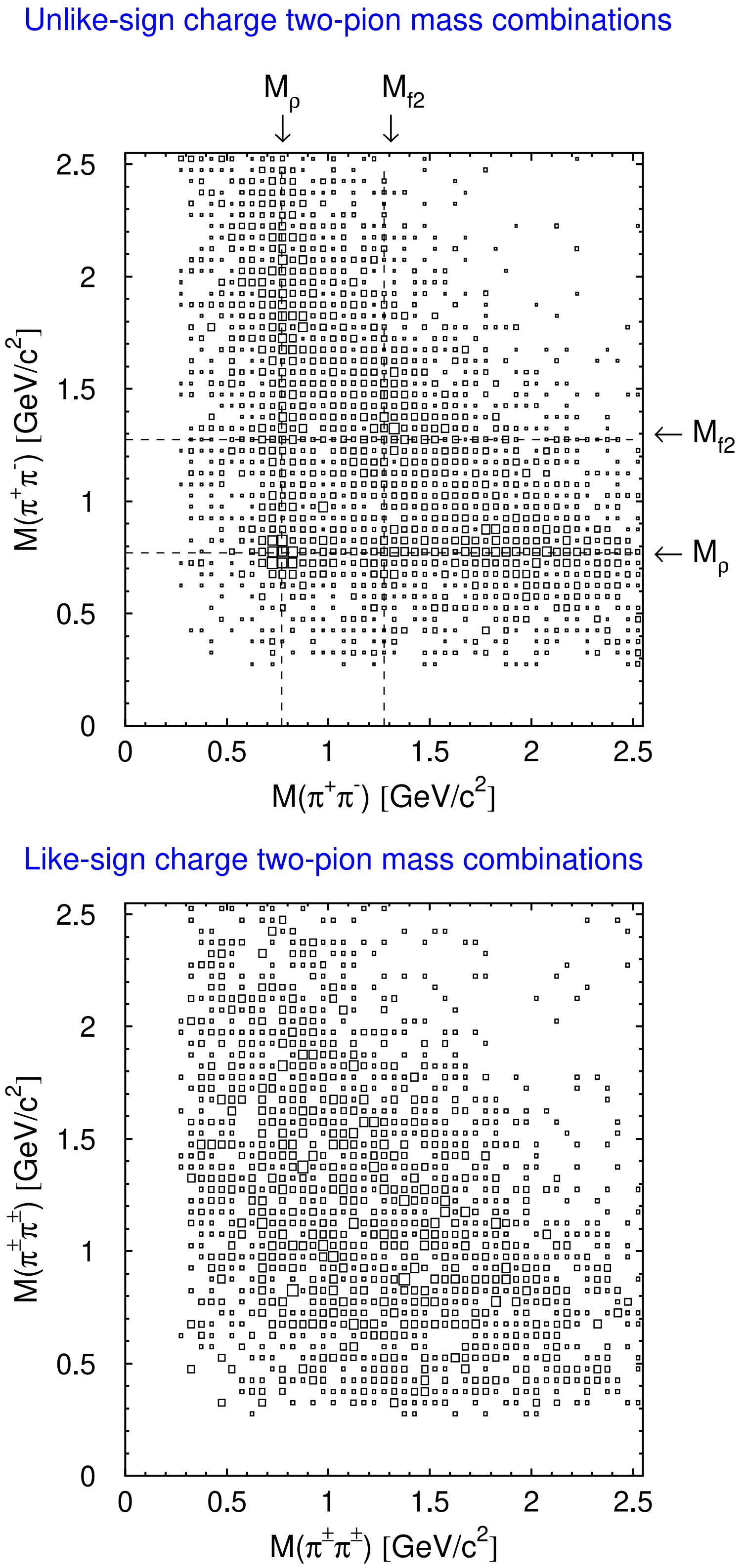

Figure 3: The same scatter plots of two pion mass distribution as on Fig. 2 but for high-mass data ($W_{\gamma\gamma} > 3.0$ GeV) Top for unlike-sign charge ($\pi^+\pi^-$) combinations (four entries per event) and bottom for like-sign charge ($\pi^\pm\pi^\pm$) mass combinations (two entries per event).

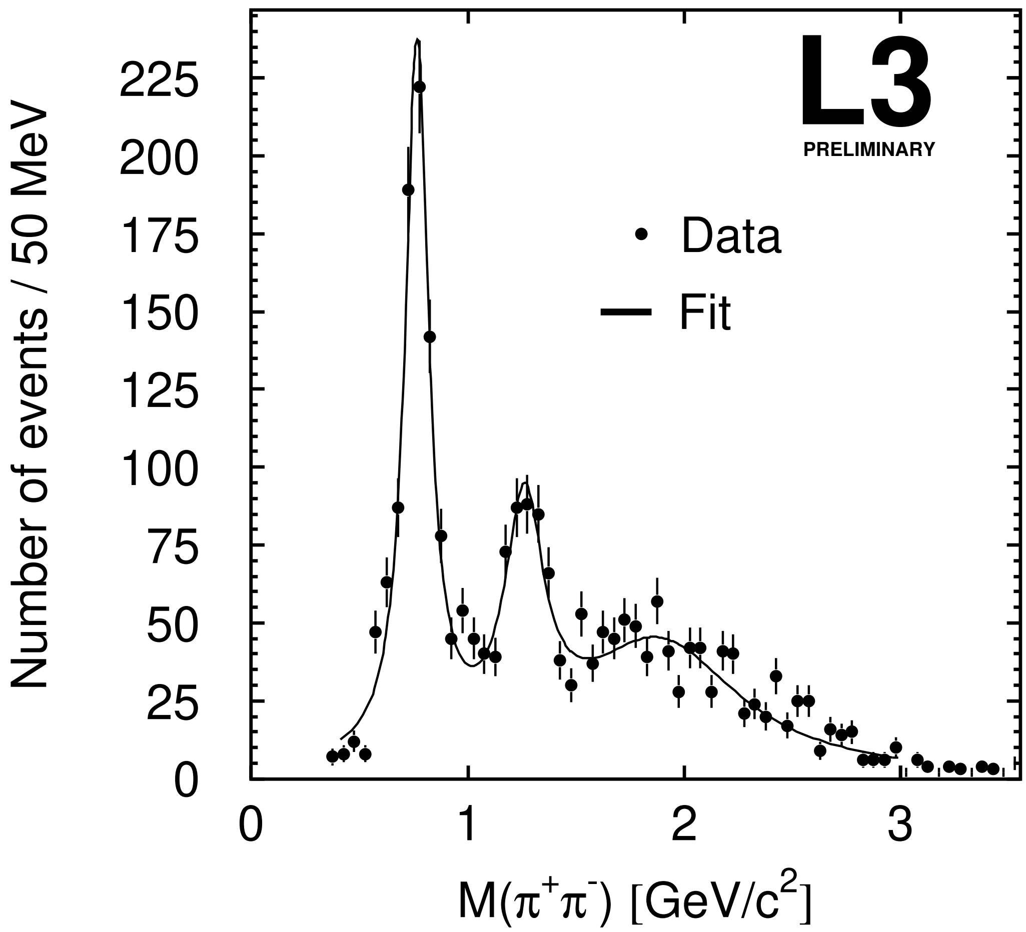

Figure 4: The two-pion mass after combinatorial background subtraction for the high mass data $W_{\gamma\gamma} > 3$ GeV.

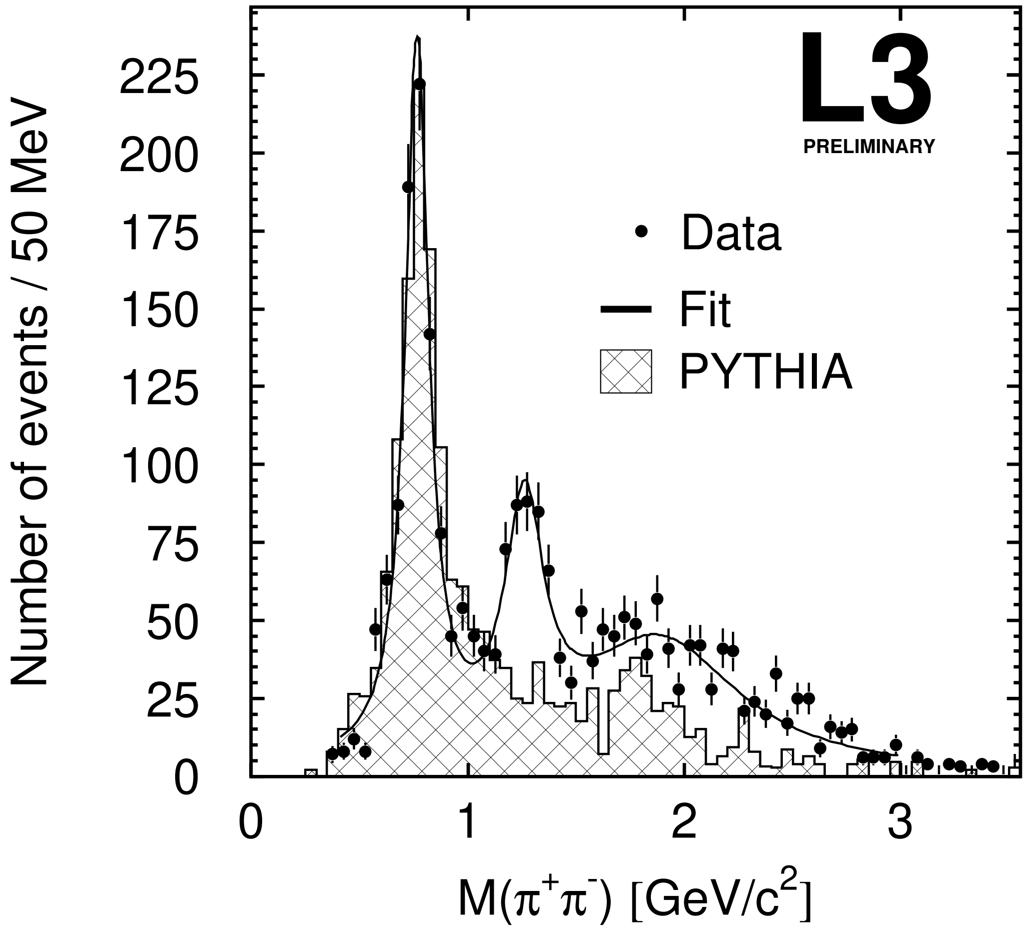

Figure 5: The two-pion mass after combinatorial background subtraction for the high mass data $W_{\gamma\gamma} > 3$ GeV compare to PYTHIA Monte Carlo prediction. PYTHIA reproduces well the shape of the ρ^0 meson, but the higher masses are missing.

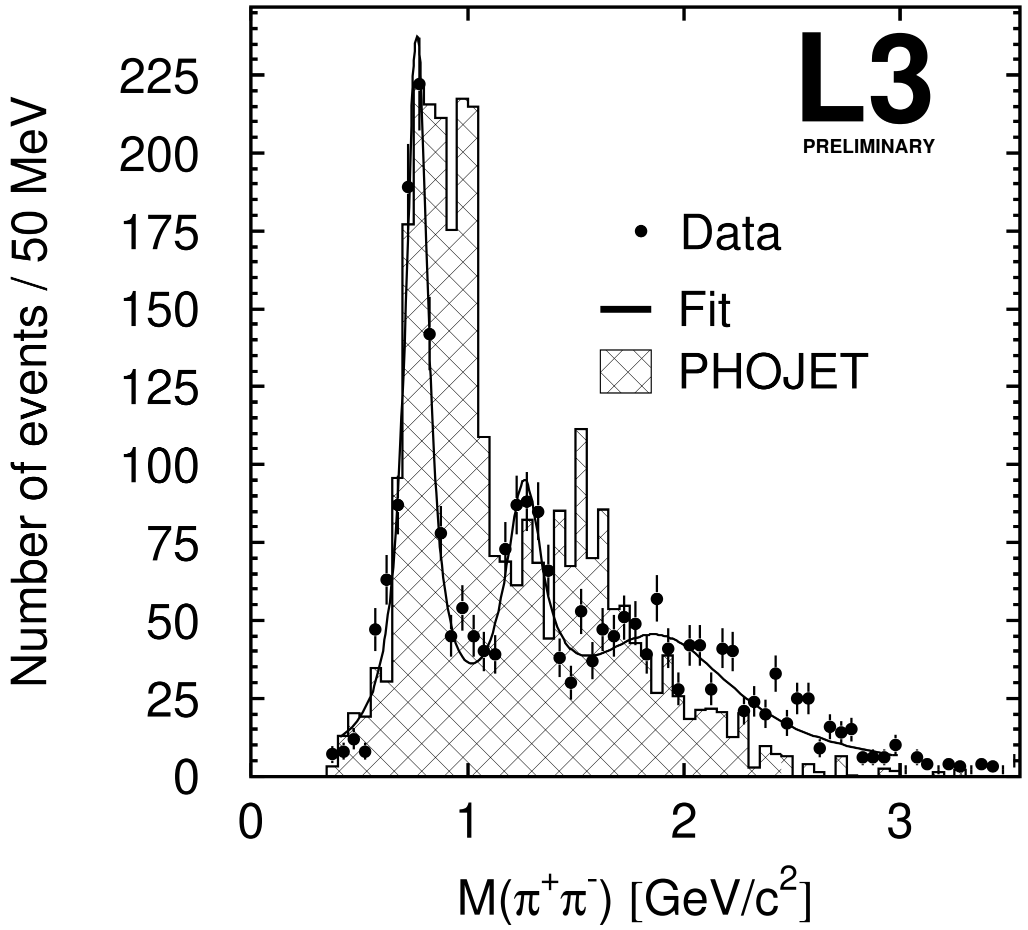

Figure 6: The two-pion mass after combinatorial background subtraction for the high mass data $W_{\gamma\gamma} > 3$ GeV compare to PHOJET Monte Carlo prediction. PHOJET has a rather smooth $\pi^+\pi^-$ spectrum with no clear resonance peak.

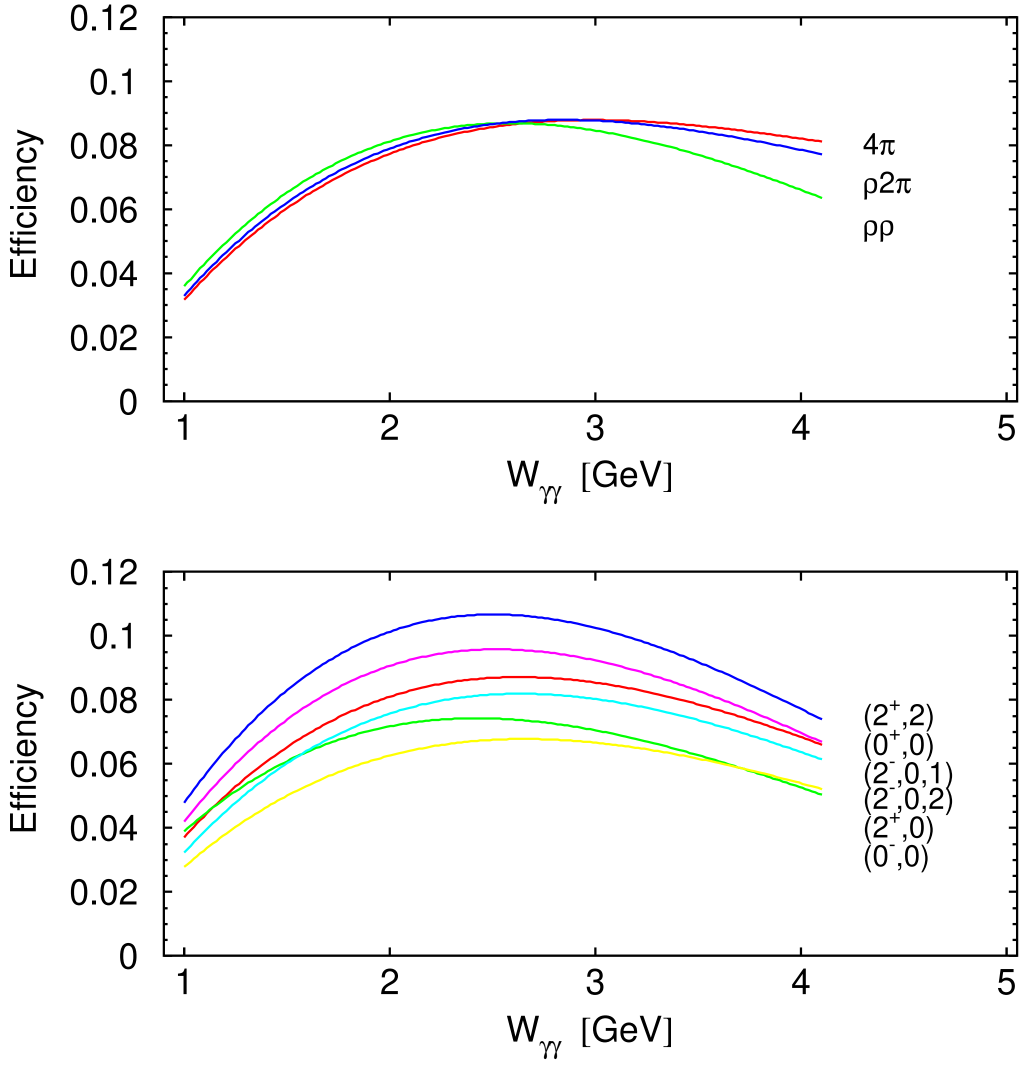

Figure 7: Selection efficiency for various $\rho^0\rho^0$ spin-parity and helicity states (J^p, J_z) (bottom) and for the isotropic $\rho^0\pi^+\pi^-$ and $\pi^+\pi^-\pi^+\pi^-$ states (top)

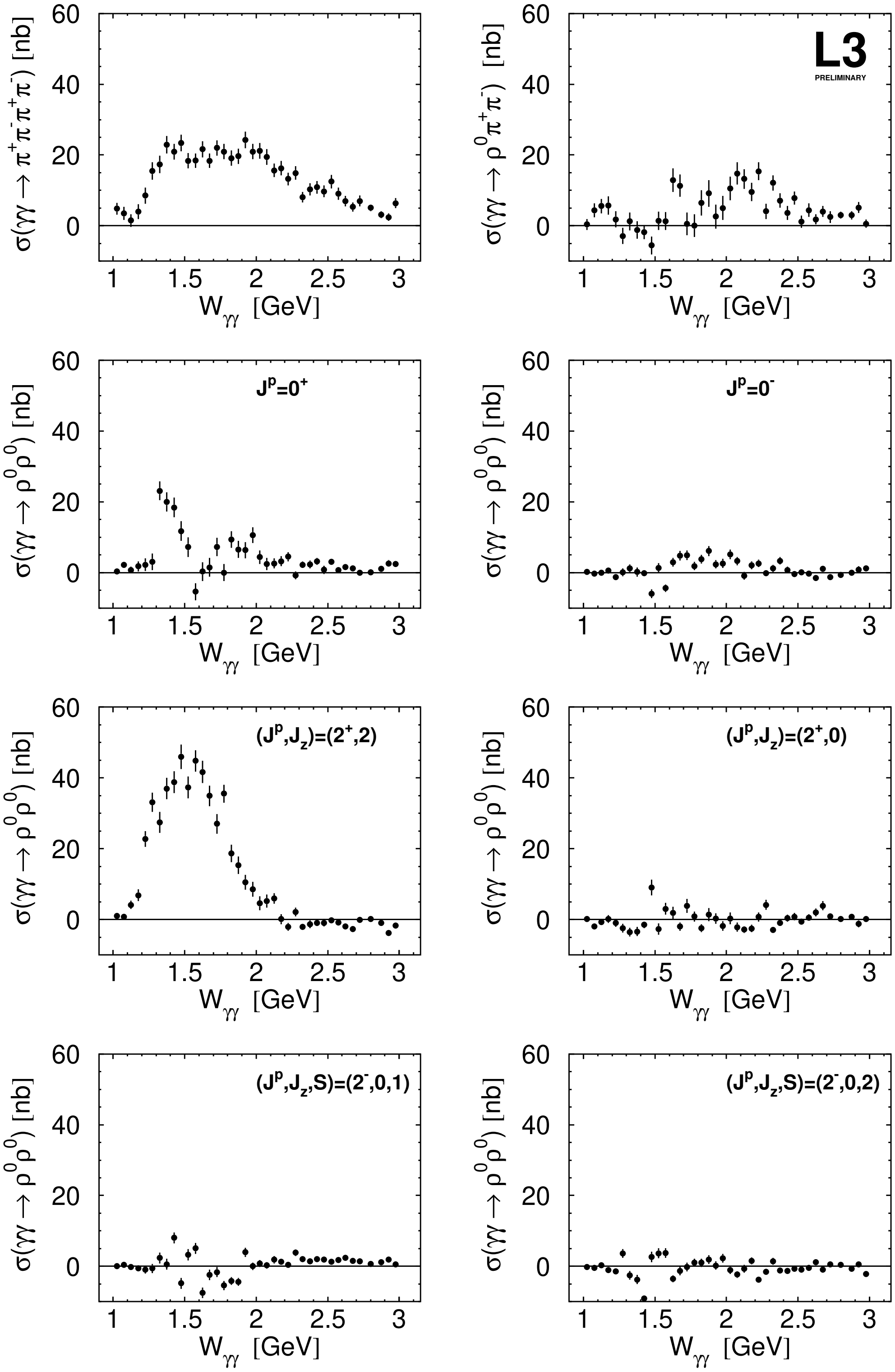

Figure 8: Cross sections for different spin-parity and helicity states (J^P, J_z) of $\rho^0\rho^0$ and for the isotropic $\rho^0\pi^+\pi^-$ and $\pi^+\pi^-\pi^+\pi^-$ states as determined by the 8 parameter fit.

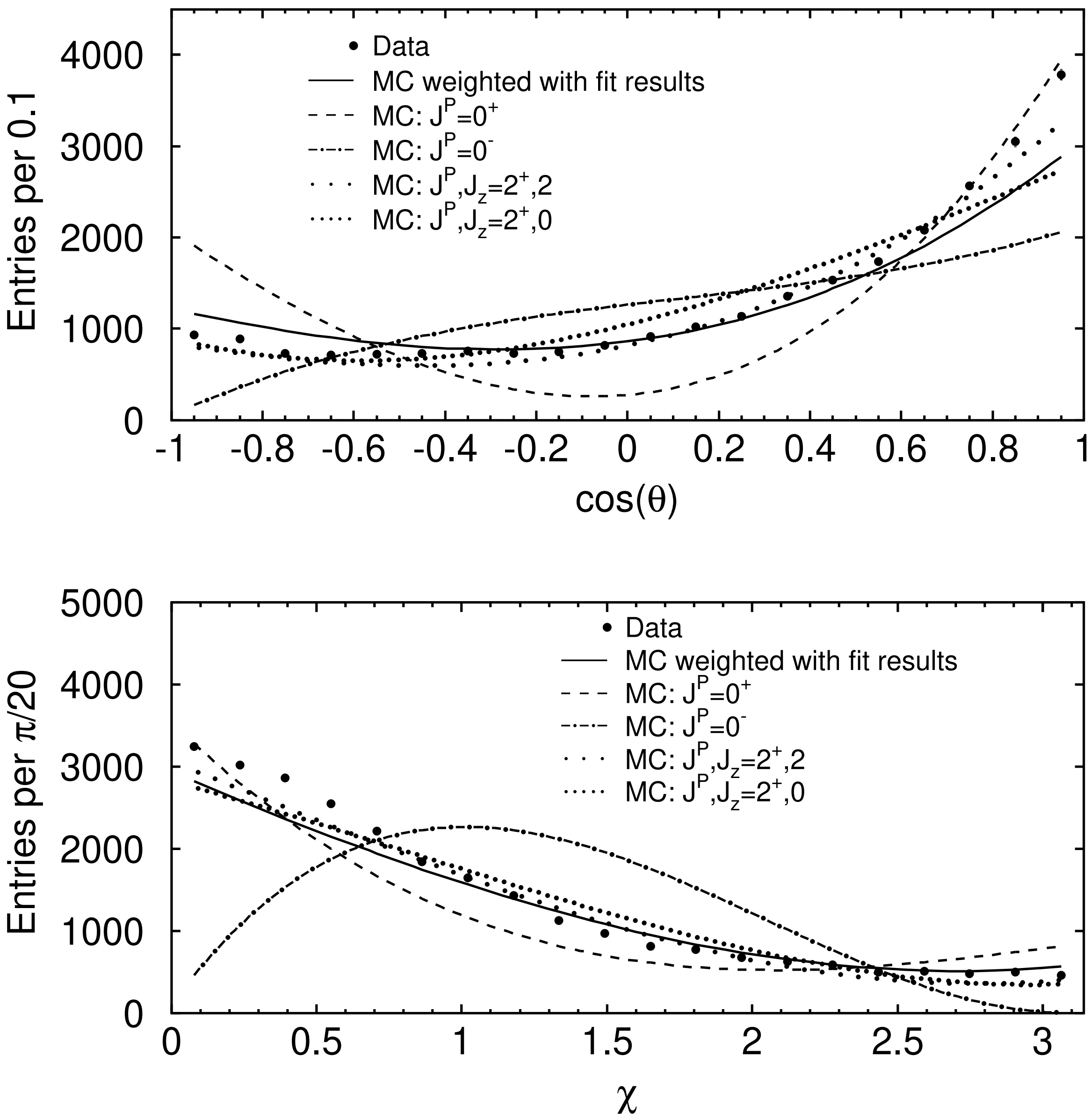

Figure 9: (up) Opening angle ϑ between two positive charged pions and (bottom) angle χ between two ρ^0 decay planes for $1.3 < W_{\gamma\gamma} < 1.5$ GeV. The result of the 8 parameter fit (solid line) is compared to the data. Also shown are the distributions for $\rho^0\rho^0$ states: $J^P = 0^+$ (dashed line), $J^P = 0^-$ (dash-dotted line), $J^P = 2^+$ with helicity 2 (dotted line) and with helicity 0 (double-dotted line).

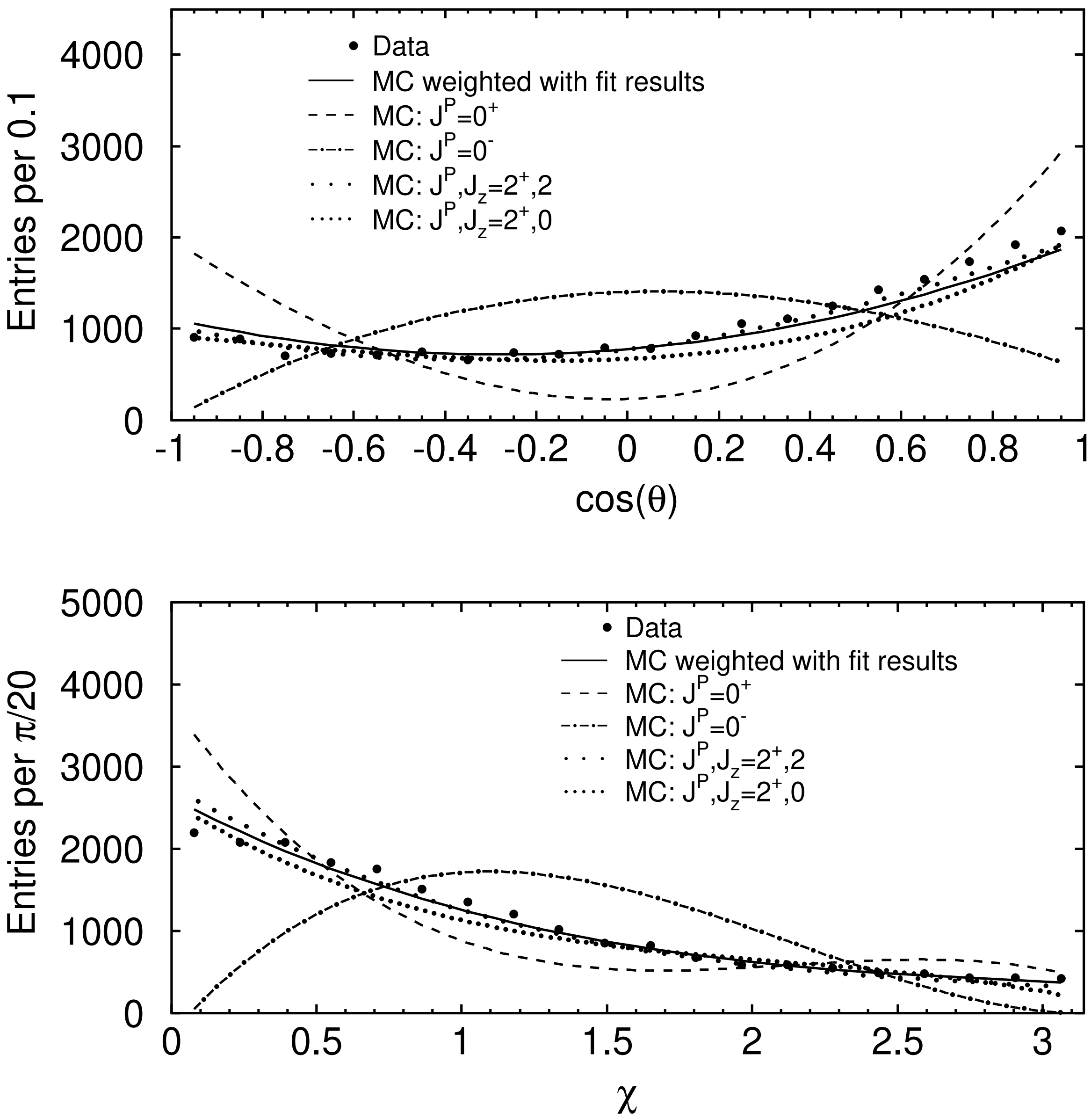

Figure 10: (up) Opening angle ϑ between two positive charged pions and (bottom) angle χ between two ρ^0 decay planes for $1.6 < W_{\gamma\gamma} < 1.8$ GeV. The result of the 8 parameter fit (solid line) is compared to the data. Also shown are the distributions for $\rho^0\rho^0$ states: $J^P = 0^+$ (dashed line), $J^P = 0^-$ (dash-dotted line), $J^P = 2^+$ with helicity 2 (dotted line) and with helicity 0 (double-dotted line).